American Mineralogist, Volume 75, pages 230–236, 1990

X-ray reference-intensity and X-ray fluorescence analyses of Salton Sea core

Briant L. Davis, Charles K. Shearer, Jr., Steven B. Simon, Michael N. Spilde, James J. Papike

South Dakota School of Mines and Technology, Rapid City, South Dakota 57701, U.S.A.

J. C. Laul

Pacific Northwest Laboratories, Battelle Memorial Institute, Richland, Washington 99352, U.S.A.

Abstract

Quantitative X-ray powder diffraction (XRD) and X-ray transmission (XRT) procedures have been combined with X-ray fluorescence (XRF) and other spectroscopic methods to characterize the mineralogy and chemistry of 33 core samples obtained from the Salton Sea Scientific Drilling Program (SSSDP) well. Major mineral components in the SSSDP samples include quartz, orthoclase, sodic plagioclase, chlorite, epidote, illite, and calcite, with minor pyrite, phlogopite, halite, anhydrite, and actinolite. Compositions of orthoclase, albite, epidote, and chlorite were determined by microprobe analysis from polished sections of SSSDP core samples for use in the XRD oxide reductions. From these mineral compositions, the weight fractions of the minerals (mineral modes) were computed from bulk chemical analyses obtained by XRF spectrometry using a least-squares minimization procedure. Measured and calculated mass-absorption coefficients were compared to locate errors in analytical parameters or in mineral chemistry. This study demonstrates the value in obtaining good bulk and individual phase chemistry for use in quantitative multicomponent X-ray diffraction analysis.

Introduction

Quantitative mineral proportions in Salton Sea core samples cannot be determined by traditional optical methods (i.e., as described by Chayes, 1956) because of the exceedingly fine grained nature of the shales and schists. This feature suggests that quantitative X-ray powder diffraction (XRD) be used. However, from an historical point of view, quantitative X-ray methods have not often been used for modal mineral determinations because of inherent difficulties in obtaining reproducible results of reasonable accuracy (Alexander, 1977). Such problems have their origin in primary extinction, microabsorption, and preferred orientation of the crystallites within all samples not having had special treatment designed to eliminate such phenomena. These difficulties are discussed by de Wolff et al. (1965), Tatlock (1966), Klug and Alexander (1974), and Cline and Snyder (1983). Tatlock overcame some of these difficulties by preparing standard mixtures from the same components found in the unknown samples, by adjusting the X-ray target output to generate quartz line intensities that matched those of such standard mixtures, and by packing the sample powders carefully in well mounts in order to eliminate at least *differences* in preferred orientation. He prepared several suites of mixtures according to mass-absorption characteristics of anticipated unknown samples; each suite consisted of mixtures with components varying at intervals of 5 wt%. Even with rapid scanning, Tatlock's reduced (i.e., summed from the individual mineral contributions) oxide compositions agreed very well with those obtained from bulk chemical analysis of sample aliquots. Maniar and Cook's (1987) granite study was a calibration approach based on quartz as a reference. Such methods require a large time expenditure but produce good results if the effort can be justified. Schultz (1964) and Muffler and White (1969) used less quantitative but faster approaches based on simple peak-height comparisons.

Recently developed sample-preparation methods that greatly reduce preferred orientation of particles have been applied to the reference-intensity-ratio method of quantitative XRD in this laboratory (Davis, 1984, 1986). Because quantitative X-ray diffraction analysis benefits so greatly from the combination of reference-intensity ratios, aerosol-suspension and filter-collection procedures, and mass-absorption-coefficient measurements, we have employed the term "reference-intensity method" (RIM) to multicomponent analysis that involves these parameters and procedures. The reference-intensity ratio (Chung, 1974a, 1974b; Hubbard et al., 1976) is a very popular parameter for use in such analyses.

The purpose of this paper is to present the results of the RIM and X-ray fluorescence (XRF) and atomic absorption–inductively coupled plasma (AA–ICP) spectroscopy analyses of 33 Salton Sea samples yielding XRD modes and associated chemical oxide tabulations that can be compared with oxides computed from the XRF–AA–ICP elemental analyses. This study is particularly valuable because of the good chemical control available for the Sal-

0003–004X/90/0102–0230$02.00

TABLE 1. Quantitative X-ray diffraction analyses, Salton Sea core

Sample*	Depth**	Qu	Or	Ab	Ch	Il	Ph	Ep	Ca	Py	Other†
First series											
4A	3014.05	31(4)	33(7)	10(1)	26(4)	—	—	—	—	0(0.07)	—
4B	3014.05	32(5)	36(7)	15(2)	16(3)	—	—	—	—	0.5(0.07)	0.6(0.15)—Ha
10A	4244.40	40(5)	34(7)	13(2)	3(1)	—	—	—	9(5)	1.5(0.2)	—
10B	4244.50	35(5)	35(7)	12(2)	5(1)	—	—	—	11(6)	1.5(0.2)	—
16A	5575.20	30(4)	26(5)	15(2)	27(4)	—	—	—	—	1.9(0.3)	—
16B	5575.50	30(4)	26(6)	15(2)	27(4)	—	—	—	—	1.9(0.3)	—
18A	6510.25	18(3)	48(8)	17(3)	17(3)	—	—	—	—	—	—
18B	6510.00	12(2)	52(8)	16(3)	20(4)	—	—	—	—	—	—
24A	7729.35	16(4)	3(1)	10(2)	13(3)	41(12)	—	—	17(9)	—	—
24B	7730.00	18(5)	—	9(2)	14(4)	47(12)	—	—	12(7)	0.8(0.2)	—
Second series											
	1561.6	22(6)	2(0.9)	2(0.6)	14(4)	49(12)	—	—	10(6)	0.2(0.04)	—
	2001.8	24(6)	3(1)	5(1)	13(3)	38(11)	—	—	17(9)	0.3(0.07)	—
	2971.0	65(5)	—	28(4)	1(0.3)	—	—	2(0.5)	3(2)	0.6(0.1)	—
	3146.9	69(7)	20(6)	3(0.6)	6(1)	—	—	—	3(2)	0.2(0.04)	—
	4678.0	52(7)	31—	1(0.2)	4(0.9)	—	—	10(1)	—	1(0.2)	—
	6040.0	21(4)	38(8)	21(3)	14(3)	—	—	—	5(3)	0.2(0.04)	—
	6511.0	70(5)	—	—	3(0.6)	—	1(1)	25(4)	—	—	2(0.9)—Mg
	6880.8	23(6)	—	11(2)	8(2)	43(11)	—	—	15(8)	1(0.2)	—
	7306.5	12(3)	42(9)	16(3)	26(5)	—	—	5(0.7)	—	—	—
	7548.3	25(5)	—	26(4)	19(4)	26(9)	—	—	4(2)	0.2(0.03)	—
	7550.2	70(5)	—	—	—	—	—	29(4)	—	—	1(0.2)—Ti
	8138.5	16(3)	27(7)	22(3)	11(2)	14(6)	—	—	9(5)	1(0.2)	—
	8395.7	22(4)	22(6)	26(4)	8(2)	18(7)	—	—	5(3)	0.2(0.04)	—
	8802.6	46(6)	5(2)	21(3)	15(3)	—	0.4(0.5)	—	12(6)	0.1(0.02)	—
	9249.3	14(3)	36(8)	38(6)	5(1)	—	6(5)	—	—	1(0.2)	—
	9249.6	0.7(0.1)	—	—	—	—	1(0.1)	72(2)	—	—	9(0.9)—Ac; 17(2)—Ah
	9474.0A	3(0.8)	28(9)	28(7)	—	—	22(5)	15(4)	—	—	4(1)—Ac
	9474.0B	9(2)	—	—	—	—	3(3)	83(3)	—	—	5(0.6)—Ac
	9474.0C	10(3)	17(6)	28(7)	—	—	23(4)	18(4)	—	—	4(1)—Ac
	9694.2	21(4)	—	58(4)	10(2)	—	—	7(0.6)	—	—	—
	9694.3	33(5)	—	54(4)	—	—	—	14(1)	—	—	—
	9907EP	48(5)	—	—	—	—	—	38(4)	—	—	13(2)—Ac; 2(0.2)—Ti
	9907SH	27(5)	29(7)	28(5)	0.6(0.1)	—	6(5)	4(0.6)	—	—	5(0.8)—Ac

Note: Values are the weight percentage of the given component; the variance errors are in parentheses. Qu = quartz. Or = orthoclase. Ab = albite. Ch = chlorite. Il = illite. Ph = phlogopite. Ep = epidote. Ca = calcite. Py = pyrite.

* A, sample taken adjacent to fracture; B, sample taken on fracture.

** Core down-hole position in feet (1 ft = 0.3048 m).

† Other phases: Ha = halite. Mg = magnetite. Ti = titanite. Ac = actinolite. Ah = anhydrite.

ton Sea samples. Considerable care in particle-size reduction, mixing, and splitting of samples was taken to ensure physically well-correlated samples, allowing adjustment of reference-intensity ratios and calculation of modes from chemical data alone. This study was one phase of a comprehensive study of the Salton Sea Scientific Drilling Project drill core (Elders and Sass, 1988). Shearer et al. (1988) have presented the petrologic significance of the mineral assemblages observed throughout the core extent.

Sample preparation

Two series of samples were analyzed from the core; the down-hole depth of each of these samples is given with the analyses in Table 1. Each sample was removed from the split core with its location marked on a photographic reproduction of the core fragments. A portion of the selected fragment was pulverized in a Spex mixer-mill for 10–20 min until a flourlike texture was achieved. Subsequent checks by optical microscopy of some of the samples demonstrated that the volumetric mean particle diameter fell within a 5- to 15-μm-diameter size range. Occasionally some samples had to be ground under alcohol to eliminate clumping.

The powdered material was suspended as an aerosol from a fluidized bed of glass microbeads and collected onto a glass fiber filter (Whatman GF/C) using the tubular aerosol-suspension chamber (TASC, Davis, 1986). Adjustment of the volume flow through the TASC may be used to limit the size of particles reaching the filter surface. The volumetric-mean particle diameter for the Salton Sea core aerosol samples fell at about 10 μm (simple mean at about 6 μm). An additional important aspect of the procedure was to ensure uniform random distribution of the particles, a prime requirement for quantitative X-ray analysis by the reference-intensity method (RIM). Additional details of this technique have been published elsewhere (Davis, 1984, 1986).

Some of the loaded filter samples were treated with ethylene glycol vapors before the samples were scanned. This treatment provided a means for separating the illite low-angle peak from that of smectite. This step was discontinued when it became apparent that the temperature at the depth of the core was sufficiently high to convert

TABLE 2. Reference-intensity ratios and mass-absorption coefficients used in Salton Sea analyses (Cu$K\alpha$ radiation)

Species	hkl	2θ	$k_i \pm$ S.D.	μ	Comments*
Quartz	101	26.65	4.0 ± 0.8	36.4	
Orthoclase	040, 002	27.50	0.7 ± 0.2	46.4	SS-16
	130	23.55	0.5 ± 0.2	46.4	SS-16
Actinolite	110	10.50	0.7 ± 0.1	63.0	
Albite	$\bar{2}02$, 002, 040	27.76	1.6 ± 0.2	34.8	SS-16
	$\bar{2}01$	22.05	0.6 ± 0.1	34.8	SS-16
Chlorite ($Fe_{3.4}$)	002	12.48	0.7 ± 0.1	72.5	SS-16
Chlorite (Fe_6)	002	12.48	1.0 ± 0.2	95.0	
Epidote	$\bar{1}02$	17.72	0.3 ± 0.01	78.3	SS-16
Illite	001	8.89	0.3 ± 0.1	49.9	M&E, 1983
Phlogopite	001	8.70	2.4 ± 0.2	50.3	
Sphene	111	27.44	1.5 ± 0.2	99.0	
Calcite	014	29.45	2.0 ± 1.2	74.3	
Pyrite	200	33.04	2.0 ± 0.2	191.1	
Magnetite	220	30.08	0.5 ± 0.2	232.1	
Anhydrite	210	31.40	1.0 ± 0.1	76.0	

* SS-16, chemical data from microprobe analysis of specific minerals. M&E, chemical data from McDowell and Elders (1983).

smectite to illite. Smectite was not observed above the limit of detection (1% by weight) in these samples; illite was distinguished from muscovite by the breadth of the 10 Å peak.

ANALYTICAL PROCEDURES

Most sample-preparation procedures were the same for both reference-intensity-ratio measurements and sample scanning. Both blank and loaded filters were weighed with a microbalance sensitive to 10 μg. Direct-beam X-ray transmission (XRT) measurements were completed on both blank and loaded filters using Cu$K\alpha$ radiation to provide mass-absorption coefficients. Following a second weighing, glycolation, and final X-ray transmission, each filter was trimmed to 2.5-cm diameter and mounted in the circular spinner mount of a Philips diffractometer. The mass-absorption *measurement* (Davis, 1984) provides a check on the composition determined by the RIM procedure via comparison with *computed* mass absorption from either the elemental or compound modes.

Reference-intensity ratios were measured for a number of mineral species for which values did not already exist. These were primarily chlorites, epidote, and actinolite. The procedure for determining a reference-intensity ratio, k_i, is essentially the same as a multicomponent analysis, except that the integrated intensities obtained are ratioed to the strong 113 corundum intensity using standard loaded in a TASC, followed by correction for sample absorption (Davis and Johnson, 1987). This process is expressed by a relationship derived by Chung (1974a),

$$k_i = \frac{[I_{i,0}][\mu_i]}{[I_{c,0}][\mu_c]} \quad (1)$$

where $I_{i,0}$ and $I_{c,0}$ are integrated intensities from pure preparations of the analyte and corundum standard, respectively, and μ_i and μ_c are the respective mass-absorption coefficients of these pure phases. Use of this procedure (rather than by mixing the phases in a 1:1 weight ratio) avoids possible differential settling of one phase relative to the other during the suspension procedure. Table 2 presents the k_i and μ_i used in all Salton Sea core analyses. With carefully controlled experimental conditions, these k_i values are exactly equivalent to those obtained with the usual 1:1 weight-mixture analysis (Hubbard et al., 1976; Davis and Johnson, 1987).

Samples were scanned at ½° 2θ min^{-1} from 4° 2θ to 45° 2θ using graphite-monochromatized Cu$K\alpha$ radiation [40 kV, 20 mA], followed by a second short scan near 56° to check for the strong pyrite peak. Intensities were integrated from either fitted Lorentzian profiles or from triangles fitted about strip-chart peaks. The intensities were then corrected for the use of automatic divergence slits and for transparency and matrix effects. These intensities, I_i, were then combined with reference intensity ratios, k_i, in the relation (Chung, 1974b)

$$W_j = \left[\frac{k_j}{I_j} \sum \frac{I_i}{k_i}\right]^{-1} \quad (2)$$

where W_j is the weight fraction of component j. All the W_j are constrained to sum to unity; the *relative* weight proportions of all analyzed components are correct regardless of the presence of unidentified components or amorphous components. However, once identified, amorphous component quantities in a sample may be determined from mass-absorption measurements if the mass-absorption coefficient of all phases, crystalline and amorphous, can be calculated or measured (Davis and Johnson, 1987). No amorphous materials were observed (by polarizing optical examination and XRD scattering) in the Salton Sea samples.

Once the mineral weight fractions (modes) are determined, all oxide and element contributions from each mineral are compiled into a table of summed values. In some cases, average values taken from literature compilations (e.g., Deer et al., 1962, 1963) were used where specific component compositions from the SSSDP pro-

gram (previously published Salton Sea work or our own measurements) were unavailable. Compositions of epidote, chlorite, albite, and orthoclase were obtained from our microprobe analyses of Salton Sea samples (Shearer et al., 1988), and illite compositions were obtained from McDowell and Elders' (1983) Elmore 1 borehole cuttings study. In a few cases, a high-Fe chlorite (Fe_6) was found to bring calculated mass-absorption coefficients closer to the observed value and was thus used in the oxide tables. Otherwise, a chlorite composition with $Fe_{3.4}$ from SS-16A (depth = 5575.2′ or 1699.3 m) determined by microprobe analysis was used.

Whole-rock powders were analyzed by several spectroscopic techniques, primarily XRF, but also AA–ICP, and flame-emission (FE) spectroscopy. Major, minor, and trace elements were analyzed by energy-dispersive XRF at the Battelle Pacific Northwest Laboratories using pressed disks of rock powder. The AA–ICP and FE analytical work made use of lithium metaborate solutions for Na, Mg, Rb, Cs, Si, and Al. In all whole-rock analyses, USGS standards BCR-1, AGV-1, G2, and GSP-1 were used. Additional details on the chemical procedures used are described by Shearer et al. (1988).

XRD QUALITY ASSURANCE AND THE ESTIMATION OF ANALYTICAL UNCERTAINTIES

Processing of the intensity data leading to the solution of Equation 2 includes a formal variance-error propagation algorithm. Errors from balance-weighing operations, transmission measurement, reference ratio (k_i) measurements, intensity measurements (including count-rate statistics), and estimated measured and calculated errors in mass absorption are all included in the method. The modal tabulations in Table 1 contain the resulting errors for each component. An assessment of the measurement variation expected for all phases of the analytical work completed by several analysts independently is presented for sample 16A in Table 3. Also included in Table 3 is the oxide reduction of the minerals compared with independent oxide analyses of chemical methods (see the section on Analytical Procedures).

Additional checking of the *precision* in measurement of μ was also made by four graduate students working independently. This group determined μ for Whatman GF/C filters to be 49.8, 48.6, 49.7, and 49.9 $cm^2 \cdot g^{-1}$, resulting in a mean of 49.5 ± 0.6 $cm^2 \cdot g^{-1}$. As an additional quality-assurance (QA) measure, the transmission intensities and weight of a CaF_2 XRT standard with calculated μ value of 95.5 $cm^2 \cdot g^{-1}$ were remeasured during the course of the analytical work on the Salton Sea core samples. The computed μ_{obs} from these measurements was 97.4 $cm^2 \cdot g^{-1}$ (2% error). Our ability to measure a mass-absorption coefficient in the range 75–100 $cm^2 \cdot g^{-1}$ with this instrument is generally within 1–2%. Routine laboratory QA measures include periodic scanning of a novaculite standard in order to make necessary instrument checks and adjustments to maintain optimum sensitivity and proper scattering-angle readings.

TABLE 3. Team analyses of Salton Sea sample 16A (depth 5575.20 ft = 1699.3 m)

Phase	RIM X-ray modal analysis (wt%)			
	Team 1	Team 2	Team 3	Mean ± S.D.
Albite (Ab_{96})	11.9	14.5	13.6	13.3 ± 1.3
Orthoclase (Or_{93})	21.5	25.5	23.1	23.4 ± 2.0
Quartz	41.7	34.3	37.5	37.8 ± 3.7
Chlorite ($Fe_{3.36}$)	22.9	23.2	24.1	23.4 ± 0.6
Pyrite	2.0	2.5	1.7	2.1 ± 0.4
μ_o ($cm^2 \cdot g^{-1}$)	52.0	49.1	50.5	50.5 ± 1.5
μ_c ($cm^2 \cdot g^{-1}$)	47.7	48.9	47.8	48.0 ± 0.7

Selected oxides	ICP	XRD reduction (wt%)			
		Team 1	Team 2	Team 3	Mean ± S.D.
CaO	1.5	0.5	0.8	0.5	0.6 ± 0.2
Fe_2O_3	7.0	6.4	5.4	6.3	6.0 ± 0.6
Al_2O_3	9.6	11.6	13.0	12.1	12.2 ± 0.7
MgO	4.0	5.2	5.3	4.2	4.9 ± 0.6
K_2O	5.2	3.7	4.3	3.9	4.0 ± 0.3

Note: Sample from same core portion as sample 16A, Table 1.

REFINEMENT PROCEDURES

Following complete RIM analysis, *measured* mass-absorption coefficients from the XRT procedure were compared with two *calculated* mass-absorption values: (1) values calculated from the XRF compositions and (2) values calculated from the RIM modes. The differences

$$D_1 = \mu_{calc,XRF} - \mu_{meas,XRT}$$
$$D_2 = \mu_{calc,RIM} - \mu_{meas,XRT}$$

were then plotted with the calculated XRF data along the abscissa and the calculated RIM data along the ordinate. An error-propagation procedure was used for computing the variance errors associated with all mass-absorption values. This procedure is based on uncertainties in measured physical parameters, such as filter-weight errors and statistical errors of counting. If these errors are represented by e_{meas} and e_{calc}, associated with μ_{meas} and μ_{calc}, respectively, the mean uncertainty is then defined as

$$\bar{E} = (\pm \bar{e}_{meas}) + (\pm \bar{e}_{calc}).$$

$\bar{E}$ was then drawn as a circle on the plot, representing the limit beyond which plotted points demonstrated major discrepancies not explained by normal experimental errors. The value of $\bar{E}$ for the set was 6.05 $cm^2 \cdot g^{-1}$. Of the 33 samples, 10 fell outside the error circle, but only 3 of these had values of D of 10 $cm^2 \cdot g^{-1}$ or greater (highest was 12.7). The largest departures from the circle appeared to reflect basic errors in composition assumptions for solid-solution minerals (e.g., chlorite, epidote) or, in a few cases, possible incorrect weights or transmission data leading to an erroneous μ_{obs}.

The second procedure used was to prepare comparative diagrams of major-oxide compositions for the XRD reductions versus the measured XRF analyses; the XRF analyses were assumed to be the more accurate. Two of these initial plots are shown in Figures 1 and 2 (dots).

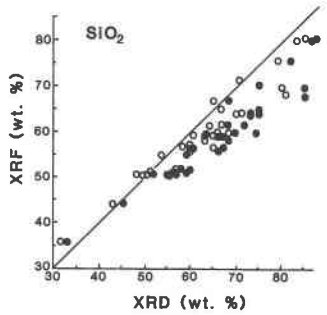

Fig. 1. SiO_2 (wt%) obtained from direct XRF analysis vs. that calculated as the sum of individual mineral contributions determined by XRD. Filled circles (dots) are initial data; open circles are values obtained following adjustment of quartz and illite reference-intensity ratios using least-squares minimization procedures (see text). Solid line gives 1:1 weight correlation.

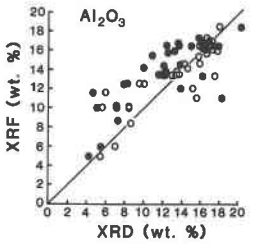

Fig. 2. Al_2O_3 (wt%) obtained from direct XRF analysis vs. that calculated as the sum of individual mineral contributions determined by XRD. Symbols as in Fig. 2. Solid line gives 1:1 weight correlation.

From these plots, it is apparent that a systematic bias exists in the data for SiO_2 and Al_2O_3.

The third procedure was to compute mineral modes from the XRF chemistry, using component compositions obtained either from literature averages or directly from microprobe analyses of mineral grains in polished thin sections. The method used (Boynton et al., 1975) was a least-squares minimization (LSM) of a matrix for each sample consisting of six phases (quartz, orthoclase, chlorite, epidote, albite, and calcite) and compositions from bulk XRF chemistry for nine elements (Si, Al, Ti, Fe^{+3}, Mn, Ca, Na, K). Although this matrix is only 80% overspecified, thus resulting in large χ^2 minima, the exercise served to demonstrate where major uncertainties in the weight fractions existed.

The reference-intensity ratio for quartz, k_q, used for many of our previous studies, was 2.84. In most of these studies, analysis was made directly on ambient filter loadings of atmospheric aerosols. The size (diameter) of particles on these filters was from 5 to 40 μm with volumetric-mean diameters estimated to be over 10 μm. In preparing reference-intensity-ratio standards in previous studies, it was not appropriate to reduce component particles to very small sizes (<5 μm). The previous quartz and calcite values were also used in studies of rock modal mineralogy with good results, as verified by independent optical analyses and/or chemical analyses. In our later analyses, it became obvious that 2.84 was too low for quartz in samples that were very finely ground. The Chung equation (Eq. 2) is self-normalizing so that absolute values of k_q cannot be determined. However, the ratio of the quartz reference-intensity ratio, k'_q, satisfying the quartz weight fraction W'_q, of the LSM set, to that used in the original analysis (k_q and W_q) may be obtained from Equation (2), i.e.,

$$\frac{k'_q}{k_q} = \frac{W_q(1 - W'_q)}{W'_q(1 - W_q)}. \qquad (3)$$

Equation 3 may then be used to determine ratios of all other k_i relative to this new value for quartz; i.e., k/k'_q, which may then be compared with our measured (RIM) ratios or ratios obtained from calculated k_i values (Borg and Smith, 1969; Jahanbagloo and Zoltai, 1968, and unpublished report, 1966). Table 4 presents the results of these computations for the original set, with $k_q = 2.84$, and the refined set with $k'_q = 4.0$ calculated from the LSM data. These tests show that, with the exception of illite, the RIM k_i ratios agree with the calculated ones much more closely when the quartz value is 4.0. The final RIM illite k_i/k_q ratio of Table 4 is still a factor of 2–3 too high, compared to calculated values, which suggests a very poorly crystalline illite in the assemblages, or some interstratification with smectite or chlorite, or both. Since illite is chemically and structurally very similar to muscovite, the calculated k_i for the $2M_1(1)$ and $2M_1(2)$ structures of Borg and Smith (1969) should not largely differ from the illite value. Consequently, for the final RIM modes, the k_i for illite was set at the average of the Borg and Smith value of 0.35, and the computed value of 0.18 (0.045 × 4.0) obtained from the LSM. Both the adjusted quartz and illite k_i values are reflected in the parameters of Table 2. Thus the illite k_i is the most uncertain parameter in the final set used; the eight samples containing illite will contain the highest uncertainties in all components, because of the self-normalizing properties of Equation 2, and they may be higher than the values given in Table 1.

Results

The final set of 33 XRD modes obtained by the RIM procedure is presented in Table 1. The values reflect the new quartz and illite k_i values and insertion of oxide compositions for those components for which specific chemical information was obtained by microprobe. The oxide abundances for the 33 samples, obtained from XRF or AA analyses, were plotted against those calculated from the XRD modes for SiO_2, Al_2O_3, Na_2O, K_2O, CaO, and Fe_2O_3, with generally good agreement. The plots of Figures 1 and 2 for SiO_2 and Al_2O_3 demonstrate the degree of improvement in correspondence after applying the quartz and illite reference-intensity-ratio corrections. There is still significant departure of the SiO_2 data from the 1:1 line;

TABLE 4. Comparison of k_i/k_q for calculated data (Borg and Smith, 1969), LSM analysis of XRF data, and initial and adjusted RIM values

	k_i/k_q					
	Or	Ab	Cℓ	Iℓ	Ca	Ep
hkl	130	$\bar{2}01$	002	001	014	$\bar{1}02$
*n**	4	7	18	6	11	6
Calculated	0.135	0.145	0.291**	0.088†	0.870	0.062
LSM	0.110	0.104	0.188	0.045	0.718	0.044
Initial RIM	0.176	0.215	0.299	0.201	0.704	0.091
Final RIM	0.125	0.153	0.212	0.143	0.500	0.065

Note: Or = orthoclase. Ab = albite. Cℓ = chlorite. Iℓ = illite. Ca = calcite. Ep = epidote.
* Number of samples included in average LSM ratios.
** Average data for corundophillite, prochlorite, ripidolite.
† Average data for $2M_1(1)$ and $2M_1(2)$ muscovites (Borg and Smith, 1969).

however, in the absence of a theoretical justification for a larger value, such further adjustment is not considered appropriate. An experimental reference-intensity ratio for randomly oriented particles of a pure phase should not exceed a calculated value since the former will contain primary extinction and microabsorption effects that reduce the k_i values, whereas the calculated value does not account for particle size–dependent parameters.

Discussion

The problems we have experienced here with the illite and quartz k_i values demonstrate how sensitive such measured values are to physical and chemical peculiarities of each phase in question. One cannot escape the fact that for a given pure-phase composition, degree of crystallinity, structure, and particle size, the k_i is truly a *universal constant*. As a practical matter, however, natural as well as laboratory-prepared samples will vary in their crystallite size and degree of crystallinity (including surface effects—Brindley and Udagawa, 1959; Altree-Williams et al., 1981), subtle compositional deviations (i.e., rutilated quartz), defect structures, and similar properties. These features, which may be induced naturally through petrogenesis, or artificially in the laboratory, can result in variable reference-intensity ratios for minerals of even simple composition. Many of these features may not be recognized by the experimentalist.

Particle size has perhaps the most important impact on quantitative XRD analysis since it affects both the k_i that is measured and the analysis of the sample itself. Particle size, extinction, and microabsorption effects are discussed by Brindley (1945), de Wolff et al. (1965), and Cline and Snyder (1983) and are appropriate to this discussion. Except for in situ filter analysis of airborne particulates (where mineral particles may attain 40- to 50-μm-diameter size in some high-volume filters), the analyst has some control over the size of particles making up the preparation. Samples with particles larger than 10 μm in diameter can show serious effects of both extinction and preferred orientation; microabsorption also becomes significant for the more highly absorbing materials. In this work the effect of particle size on the k_i for quartz used in previous airborne particulate analyses is apparent. These effects have also been discussed by Klug and Alexander (1974, p. 366). For samples with mean particle diameters below 10 μm, the quartz k_i should be about 4, near the calculated value, unless other physical or chemical peculiarities are present. The illite k_i uncertainties discussed may be due to integrated intensity-measurement errors and possibly to poor crystallinity (but not to stacking disorder, which will not affect 00l reflections from the ordered phase).

Conclusions

This study represents a comprehensive application of RIM quantitative analysis to mineralogically complex samples. Variations in reference-intensity ratios can result from both variations in particle size of the prepared sample as well as from petrogenesis, and therefore the accuracy of modal mineralogies of rocks such as those studied here can be improved by the use of chemical data and mass-absorption measurements. After applying the adjustments to the quartz and illite k_i values made possible by XRF and mass-absorption observations, the agreement between XRD-reduced oxides and those obtained directly by XRF analysis for the Salton Sea core samples is good. At least minor variations in k_i due to petrogenesis will always have to be dealt with in the analysis of natural rocks.

The RIM method of analysis provides several advantages in a study of this type: (1) a unique sample-preparation procedure designed to greatly reduce preferred orientation of particles, (2) mass-absorption-coefficient determination that provides a means for thin-layer intensity correction and a check on composition determined from optical and X-ray modes or chemical elemental analyses, and (3) error propagation for locating sources of input error. The availability of chemical data for the rock samples and microprobe data for several of the mineral phases has also permitted a least-squares minimization determination of phase weight fractions. X-ray modal analyses have made possible the assignment of probable mineral reactions leading to the observed assemblages that compose the three metamorphic zones of the sedimentary column sampled by the Salton Sea core (Shearer et al., 1988). RIM analysis is ideally suited as the means

for obtaining such modes in fine-grained sedimentary rocks and their metamorphic derivatives.

Acknowledgments

This research was conducted under the sponsorship of the Department of Energy, Grant No. DE-FG01-85ER13407, as part of the Salton Sea Scientific Drilling Project.

References cited

Alexander, L.E. (1977), Forty years of quantitative diffraction analysis. Advances in X-ray Analysis, 20, 1–13.

Altree-Williams, S., Byrnes, J.G., and Jordan, B. (1981) Amorphous surface and quantitative X-ray powder diffractometry. Analyst, 106, 69–75.

Borg, I.Y., and Smith, D.K. (1969) Calculated X-ray powder patterns for silicate minerals. Geological Society of America Memoir 122.

Boynton, W.V., Baedecker, P.A., Chou, C.-L., Robinson, K.L., and Wasson, J.T. (1975) Mixing and transport of lunar surface materials: Evidence obtained by the determination of lithophile, siderophile, and volatile elements. Proceedings, 6th Lunar Science Conference, vol. 2, Chemical and isotopic studies, p. 2241–2259. Pergamon Press, New York.

Brindley, G.W. (1945) The effect of grain or particle size on X-ray reflections from mixed powders and alloys, considered in relation to the determination of crystalline substances by X-ray methods. Philosophical Magazine, 36, 347–369.

Brindley, G.W., and Udagawa, S. (1959) Sources of error in the X-ray determination of quartz. Journal of the American Ceramic Society, 42, 643–644.

Chayes, F. (1956) Petrographical modal analysis. Wiley, New York.

Chung, F. (1974a) Quantitative interpretation of X-ray diffraction patterns of mixtures. I. Matrix flushing method for quantitative multicomponent analysis. Journal of Applied Crystallography, 7, 519–525.

——— (1974b) Quantitative interpretation of X-ray diffraction patterns of mixtures. II. Adiabatic principle of x-ray diffraction analysis of mixtures. Journal of Applied Crystallography, 7, 526–531.

Cline, J.P., and Snyder, R.L. (1983) The dramatic effect of crystallite size on X-ray intensities. Advances in X-ray Analysis, 26, 111–117.

Davis, B.L. (1984) Reference intensity quantitative analysis using thin-layer aerosol samples. Advances in X-ray Analysis, 27, 339–348.

——— (1986) A tubular aerosol suspension chamber for the preparation of powder samples for X-ray diffraction analysis. Powder Diffraction, 1, 240–243.

Davis, B.L., and Johnson, L.R. (1987) The use of mass absorption in quantitative X-ray diffraction analysis. Advances in X-ray Analysis, 30, 333–342.

Deer, W.A., Howie, R.A., and Zussman, J. (1962, 1963) Rock-forming minerals, vols. 1–5. Wiley, New York.

de Wolff, P.M., Taylor, J.M., and Parrish, W. (1965) Experimental study of effect of crystallite size statistics on X-ray diffractometer intensities. Journal of Applied Physics, 30, 63–69.

Elders, W.A., and Sass, J.H. (1988) The Salton Sea Scientific Drilling Project. Journal of Geophysical Research, 93, 12,953–12,968.

Hubbard, C.R., Evans, E.H., and Smith, D.K. (1976) The reference intensity ratio, I/I_c, for computer simulated powder patterns. Journal of Applied Crystallography, 9, 169–174.

Jahanbagloo, C., and Zoltai, T. (1968) Quantitative analysis with the aid of calculated X-ray powder patterns. Analytical Chemistry, 40, 1739–1741.

Klug, H.P., and Alexander, L.E. (1974) X-ray diffraction procedures. Wiley, New York.

Maniar, P.D., and Cook, G.A. (1987) Modal analyses of granitoids by quantitative X-ray diffraction. American Mineralogist, 72, 433–437.

McDowell, S.D., and Elders, W.A. (1983) Allogenic layer silicate minerals in borehole Elmore #1, Salton Sea geothermal field, California. American Mineralogist, 68, 1146–1159.

Muffler, L.J.P., and White, D.E. (1969) Active metamorphism of upper Cenozoic sediments in the Salton Sea geothermal field and the Salton Sea trough, southeastern California. Geological Society of America Bulletin, 80, 157–182.

Schultz, L.G. (1964) Quantitative interpretation of mineralogical composition from X-ray and chemical data for the Pierre Shale. U.S. Geological Survey Professional Paper 391-C, 31 p.

Shearer, C.K., Papike, J.J., Simon, S.B., Davis, B.L., and Laul, J.C. (1988) Mineral reactions in altered sediments from the California State 2-14 well: Variations in the modal mineralogy, mineral chemistry, and bulk composition of the Salton Sea Scientific Drilling Project Core. Journal of Geophysical Research, 93, 13,104–13,122.

Tatlock, D.B. (1966) Rapid modal analysis of some felsic rocks from calibrated X-ray diffraction patterns. U.S. Geological Survey Bulletin, 1209, 41 p.

Manuscript received September 23, 1988
Manuscript accepted September 29, 1989